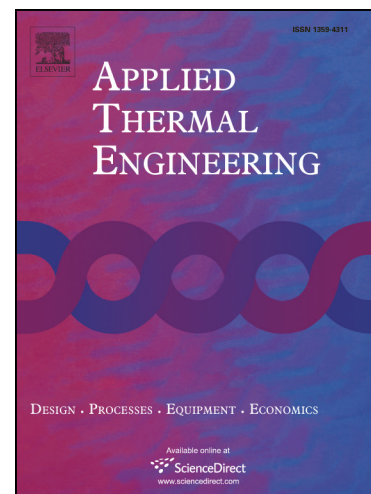# Accepted Manuscript

A novel effective thermal conductivity correlation of the PCM melting in spherical PCM encapsulation for the packed bed TES system

Zhirong Liao, Chao Xu, Yunxiu Ren, Feng Gao, Xing Ju, Xiaoze Du

Please cite this article as: Z. Liao, C. Xu, Y. Ren, F. Gao, X. Ju, X. Du, A novel effective thermal conductivity correlation of the PCM melting in spherical PCM encapsulation for the packed bed TES system, *Applied Thermal Engineering* (2018), doi: https://doi.org/10.1016/j.applthermaleng.2018.02.048

A novel effective thermal conductivity correlation of the PCM melting in spherical PCM encapsulation for the packed bed TES system

Zhirong Liao[1,2], Chao Xu[1*], Yunxiu Ren[1], Feng Gao[2], Xing Ju[1], Xiaoze Du[1]

[1]State Key Laboratory of Alternate Electrical Power System with Renewable Energy Sources, North China Electric Power University, Beijing 102206, China

[2]Beijing Shouhang IHW Resources Technology Co., Ltd, Beijing 100070, China

*Corresponding author. Tel.: +86 10 61773934; fax: +86 10 61773877.

E-mail address: mechxu@ncepu.edu.cn (C. Xu)

Abstract

Packed bed thermal energy storage (TES) system with phase change material (PCM) encapsulation is one of the potential TES technologies for the solar thermal application. In present study, the constrained melting process of PCM in spherical encapsulation is simulated by a validated natural convection included model. This model is then used to simulate the melting processes of $NaNO_3$ with different conditions. Meanwhile, the same melting processes are also calculated by the conduction controlled model with available effective thermal conductivity correlations reported in the literature. It is found that the changes of liquid fraction obtained from the natural convection included model and the conduction controlled model with the reported thermal conductivity correlations shows

1

obvious difference. Then, based on the simulating results of the cases using the natural convection included model, a new correlation for the effective thermal conductivity is proposed by linear regression. It shows that the conduction controlled model with the proposed effective thermal conductivity correlation gives better results on the change of liquid fraction than that with correlations reported in the literature. Therefore, the proposed correlation can be used to calculate the melting process of PCM in a capsule by the conduction controlled model, which is in urgent need for modeling of packed bed latent TES systems.

Keywords: packed bed thermal energy storage; effective thermal conductivity; phase change material; melting process; numerical simulation

1. Introduction

Thermal energy storage (TES) is of great interest in solar thermal applications. For example, TES can significantly improve the flexibility and dispatchability of the concentrated solar power plant [1]. According to the heat storage mechanism, TES can be divided into sensible heat storage, latent heat storage, and thermochemical storage [2]. In sensible TES system, thermal energy is stored/released by raising/lowering the temperature of the storage medium without phase change or chemical reaction. Latent TES system absorbs/releases thermal energy through phase change process. Thermochemical TES system stores or releases thermal energy by a reversible sorption or chemical reaction. Even though thermochemical TES system shows great potential, it is

still at the very early stage of development. Sensible TES system is the most matured one, but it usually suffers from low heat storage density. Recently, latent TES technology is attracting more and more worldwide attentions due to its high heat storage density and transferring heat at nearly constant temperature.

A packed bed latent TES system consists of small encapsulated PCM particles through which a heat transfer fluid (HTF) is circulated and thermal energy is transferred during the charging and discharging processes [3]. The packed bed latent TES system can achieve a much more compact storage system than sensible TES system, and overcome the low charging/discharging rate, attributed to the low PCM thermal conductivity, by increasing the specific heat exchanging area. For instance, the packed bed latent TES system (or one tank thermocline TES with PCM material) gains increasing attention for the commercial CSP plant due to the potential lower cost comparing with the two tank TES system [4].

Many numerical simulation efforts have been focused on the parametric studies and the overall thermal performance of the packed bed latent TES system. Due to the complex geometry and huge computational cost, it is very hard to directly simulate the overall packed bed system in three dimension. Hence, most mathematical models for the packed bed system are simplified to be one or two dimension [5, 6]. In addition, during the PCM melting process in a capsule, the buoyancy-driven natural convection occurs between the solid-liquid interface and the inner wall of the capsule shell. Thus, different from the solidification process which is ruled by heat conduction, the melting process is dominated by the natural convection [7]. Actually, there are two types of PCM melting within a spherical capsule: unconstrained and constrained [8]. Unconstrained melting

3

means the unmelted solid PCM can migrate due to the density difference between the solid and liquid phases [9], while constrained melting means the solid PCM will hold its position during the melting process [7, 8, 10, 11]. To simplify the simulating complexity of the melting process, heat transfer in capsules is typically represented by a conduction controlled energy equation and the natural convection inside is not directly considered. Instead, an effective thermal conductivity of liquid PCM is introduced to incorporate the effect of both heat conduction and natural convection.

The effective thermal conductivity was used to simulate the melting process in a single capsule. Bedecarrat et al. [12] used an effective thermal conductivity of 1.1 W m^{-1} K^{-1} for water melting in a capsule with a diameter of 7.3 cm. While, in the numerical work of Ismail et al. [13], the effective thermal conductivity of water was set to be 2.5 W m^{-1} K^{-1} for the sphere capsules with a diameter of 12 cm. Amin et al. [14] showed that the effective thermal conductivity of water was about 1.8-3.5 times of the water thermal conductivity during the melting process with Rayleigh number ranging from 6.8×10^{6} to 4.4×10^{7}.

More importantly, the effective thermal conductivity was widely used in the numerical models to simulate the dynamic performance of the packed bed latent TES system. In the study of Karthikeyan et al. [15], the effective thermal conductivity of PCM (paraffin wax) is set to be 0.4 W m^{-1} K^{-1} , which is twice as large as its original thermal conductivity, and by an enthalpy based model the charging process for a packed-bed TES system with PCM capsules was analyzed. Bellan et al. [16] used the Raithby and Holland's correlation [17] to calculate the effective thermal conductivity of nitrate sodium (NaNO$_3$) and numerically study the influences of capsule size and HTF flow rate

4

on the thermal performance of a packed-bed latent TES system. The formula for the effective thermal conductivity of PCM presented in [5] was cited in Refs. [18, 19] and a dispersion-concentric (D-C) model was used to investigate the dynamic thermal performance of a molten salt packed bed latent TES system and the cyclic behaviors of a packed-bed TES filled with cascaded PCM capsules. The correlation developed by Scanlan et al. [20] was used by Kalaiselvam et al. [21] to study the phase change process and the thermodynamic behavior in the capsule enclosed PCM with dispersion of nanoparticles and the cyclic performance of the packed bed latent TES system.

According to Holman's work [22], the effective thermal conductivity of free convection in enclosures follows the general form:

$$\frac{k_{eff}}{k} = C\left(Gr_{\delta}\,\mathrm{Pr}\right)^{m}\left(\frac{L}{\delta}\right)^{n} \tag{1}$$

where k_{eff} and k are the effective thermal conductivity and the PCM thermal conductivity, respectively; C, m and n are constants, and δ is the gap spacing. The effective thermal conductivity correlations for natural convection inside spherical enclose reported in the literature are listed in Table 1. Base on the natural convection experiments between two concentric spheres of four fluids includes water, air, Dow-Corning 200 Fluid-20 CS and Dow-Corning 200 Fluid-350 CS, Scanlan et al. [20] developed Eqs. (2) and (3). Scanlan et al. [20] recommended Eq. (2) for $1.2\times10^{2}< Ra_{\delta}\,\delta/r_{i} <1.1\times10^{9}$, $0.7<Pr<4148$, and $0.09<\delta/r_{i}<1.81$, while Eq. (3) was cited by [21, 23] to calculate the heat transfer inside a PCM capsule. After summarizing available reported experimental data in Weber et al. [24] and Scanlan et al. [20], Raithby and Hollands [17] proposed Eq. (4) for free convection between two concentric spheres considering the geometries effects. Chiu and Chen [25]

5

investigated the natural convection between concentric and vertically eccentric spheres and presented Eq. (5) which was used to simulate the melting process in a spherical capsule with PCM in Xia et al. [5]. It should be noted that the characteristic length of the *Ra* number in Eq. (5) is the capsule radius (r_i) instead of δ. In 2014, based on the experimental and numerical simulating results, Amin et al. [14] proposed Eq. (6) to calculate the effective thermal conductivity for water melting in a sphere with Ra_{r_i} ranging from 6.8×10^6 to 4.4×10^7.

Table 1 Effective thermal conductivity equations for natural convection inside spherical enclosures.

Eq.	Effective thermal conductivity, k_{eff}	Ref.
(2)	$\dfrac{k_{eff}}{k} = 0.228(Ra_\delta \dfrac{\delta}{r_i})^{0.226}$	[20]
(3)	$\dfrac{k_{eff}}{k} = 0.202(Ra_\delta)^{0.228}\left(\dfrac{\delta}{r_i}\right)^{0.252} Pr^{0.029}$	[20, 21, 23]
(4)	$\dfrac{k_{eff}}{k} = 0.61\left[\dfrac{\delta}{(d_o d_i)^4} \dfrac{Ra_\delta}{(d_i^{-7/5} + d_o^{-7/5})^5}\right]^{1/4}$	[16, 17]
(5)	$\dfrac{k_{eff}}{k} = 0.18(Ra_{r_i})^{0.25}$	[5, 25, 26]
(6)	$\dfrac{k_{eff}}{k} = \left(3.8475 \times 10^{-8}\right)Ra_{r_i} + 1.5859$	[14]

It can be seen that the above described equations have their own validated range in Rayleigh number and Prandtl number. Besides, except Eq. (6) all the equations were deduced without phase change phenomenon. It should be noted that Eq. (6) was developed by using water as PCM, but water contracts during the melting process which is different

6

from most other available PCMs. Therefore, these equations were not developed for the melting process inside a capsule for the most available PCMs for TES [27]. Whether these above mentioned equations can be used to correctly simulate the melting of high temperature PCM like molten salt in a spherical capsule remains unknown.

To address this knowledge gap, present study firstly presents a natural convection included model to simulate the constrained melting process in a spherical capsule. This model is then validated by comparing with the experimental results in the literature. In addition, this model is used to simulate the melting processes of the sodium nitrate under different geometric and thermal conditions. Simultaneously, the same melting processes are calculated by the conduction controlled model with the available effective thermal conductivity correlations (Eqs. (2-6)). By comparing the results from the natural convection included model and the conduction controlled model, the accuracy of the effective thermal conductivity correlations is discussed. Finally, a new correlation for the effective thermal conductivity with better accuracy is proposed.
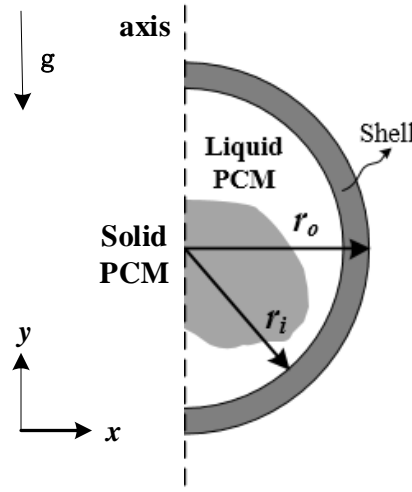
2. Mathematical modeling and validation

Fig. 1 Schematic diagram of a single PCM capsule during the melting process.

The melting process of a single PCM capsule is simulated in this section. As shown in Fig. 1, nitrate sodium ($NaNO_3$) is used as the PCM, and it is encapsulated by a spherical capsule shell. Due to the axial symmetry, the physical domain can be simplified to be a two dimensional model. Due to the buoyancy-driven convection, the solid-liquid interface of PCM is not roundish. Some simplifications or assumptions are employed in the simulation, including: (1) the outer surface of the capsule shell is assumed to be a constant wall temperature boundary; (2) the constrained melting process is considered, and the PCM density is assumed to be constant during the melting process.

The solid-liquid phase change during the melting process is calculated by the enthalpy method [28], and the Boussinesq approximation is used to deal with the natural convection. The governing equations to simulate the melting process are described as follows.

Continuity equation:

8

$$\frac{\partial u}{\partial x}+\frac{\partial v}{\partial y}=0 \tag{7}$$

Momentum equations:

x-direction:

$$\rho\left(\frac{\partial u}{\partial t}+u\frac{\partial u}{\partial x}+v\frac{\partial v}{\partial y}\right)=-\frac{\partial P}{\partial x}+\mu\left(\frac{\partial^2 u}{\partial x^2}+\frac{\partial^2 u}{\partial y^2}\right)-Cu\frac{(1-f)^2}{f^3+\varepsilon} \tag{8}$$

y-direction:

$$\rho\left(\frac{\partial v}{\partial t}+u\frac{\partial v}{\partial x}+v\frac{\partial v}{\partial y}\right)=-\frac{\partial P}{\partial y}+\mu\left(\frac{\partial^2 v}{\partial x^2}+\frac{\partial^2 v}{\partial y^2}\right)-Cv\frac{(1-f)^2}{f^3+\varepsilon}+\rho_{ref}g\beta\left(T-T_{ref}\right) \tag{9}$$

where C is the mushy zone constant. To prevent division on zero where the liquid fraction f is zero, a small parameter ε (=0.001) is added on the denominator of the third terms on the right-hand side of Eqs. (8) and (9). The liquid fraction f is calculated by:

$$f=\begin{cases}1 & T\geq T_l\\ \dfrac{T-T_s}{T_l-T_s} & T_s>T>T_l\\ 0 & T\leq T_s\end{cases} \tag{10}$$

where T_l and T_s are the liquidus and solidus temperature of the PCM, respectively.

Energy equation of the PCM:

$$\rho C_p\left(\frac{\partial T}{\partial t}+u\frac{\partial T}{\partial x}+v\frac{\partial T}{\partial y}\right)=k\left(\frac{\partial^2 T}{\partial x^2}+\frac{\partial^2 T}{\partial y^2}\right)-\rho\Delta H\frac{\partial f}{\partial t} \tag{11}$$

where ΔH is the latent heat of the PCM.

Energy equation of the capsule shell:

$$\rho_s C_{p,s}\frac{\partial T}{\partial t}=k_s\left(\frac{\partial^2 T}{\partial x^2}+\frac{\partial^2 T}{\partial y^2}\right) \tag{12}$$

9

During the melting process, the temperature of the shell outer surface is fixed to T_o, which is higher than the liquidus temperature of the PCM. The interface between the inner surface of the shell and the PCM is coupled for equilibrium of temperature and energy balance with no-slip condition. The initial temperature of the shell capsule and the PCM is T_{ini}, which is lower than the melting point of the PCM. The mushy zone constant C is set to be 10^5 kg m^{-3} s^{-1} [7].

The properties of the PCM (NaNO$_3$) and the shell material (steel) are shown in Table 2. Other properties of NaNO$_3$ include the melting temperature of 579 K, the latent heat of 178 kJ kg^{-1}, and the thermal expansion coefficient of 3.83×10^{-4} K^{-1} [29, 30]. In the simulation, the liquidus temperature is 0.1 K higher than the melting temperature while the solidus temperature is 0.1 K lower than the melting temperature.

Table 2 Material properties of NaNO$_3$ and steel.

Material		ρ (kg m^{-3})	c_p (J kg^{-1} K^{-1})	k (W m^{-1} K^{-1})	μ (Pa s)
NaNO$_3$	Solid	2150	1740	0.68	N/A
	Liquid	2150	1680	0.55	0.00289
Steel	Solid	8030	502	16.3	N/A

The above mentioned mathematical model (natural convection included model, termed as Model 1 hereafter) is then used to simulate the melting process of NaNO$_3$ inside a steel capsule with an inner diameter of 5.0 cm and a shell thickness of 0.2 cm. The Rayleigh number is lower than 10^9, so the natural convection in the capsule is laminar. The SIMPLE algorithm is used for the pressure-velocity coupling. The spatial discretization of momentum and energy are second order upwind accuracy. The residual

convergence criteria for the continuity, velocity, and energy are 10^{-3}, 10^{-4}, and 10^{-6}, respectively. To achieve the grid and time-step independences, results of different time-steps (0.2 s, 0.1 s, 0.05 s, 0.025 s, 0.01s) and different cell elements (4080, 5280, 9120, 17800, 34950) are checked. Finally, the 0.025 s time-step and 17800 cell elements are adopted. It should be emphasized that the time-step and grid independences are also checked for other capsules with different sizes discussed in the following section.

In order to validate the above model, the model is used to simulate an experiment conducted by Fan et al. [10]. In that experiment, PCM (*n*-octadecane) was filled into a spherical capsule which was made of Plexiglas. Properties of PCM and Plexiglas are the same as that in Fan et al. [10]. Fig. 2 shows the comparison of the liquid fraction during the melting process obtained from the reported experiment and Model 1. It can be seen that the predicted result of Model 1 agrees well with the experimental result, and the deviation is smaller than 3%. Therefore, Model 1 can be used to calculate the melting process in a capsule.
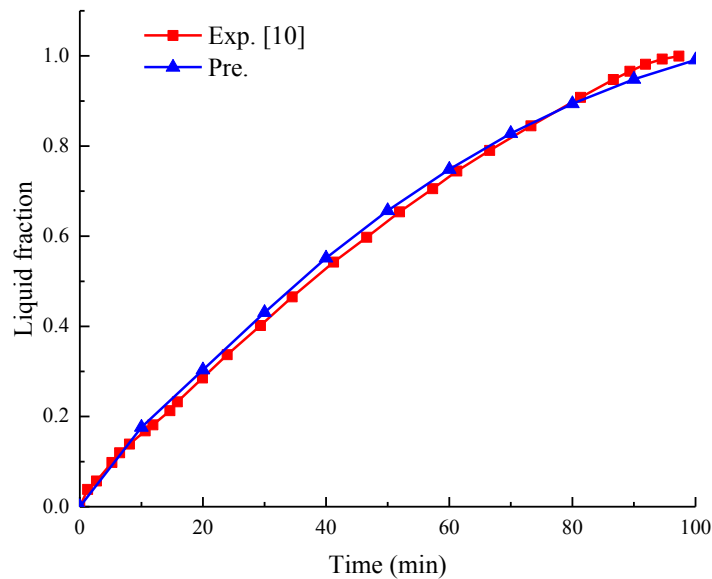

11

Fig. 2 Comparisons of the liquid fraction during the melting process between the reported

result (Exp. [10]) and the simulating result of present Model 1(Pre.).

3. Results and discussion

Since the heat transfer during the PCM melting process under different conditions is similar, a specific case (Case 1) is discussed with T_o=600 K, r_o=5.2 cm, r_i=5.0 cm, and T_{ini}=578 K. Fig. 3 shows the evaluation of the liquid fraction (left) and the streamlines (right) of $NaNO_3$ during the melting process. The red color portion of the left part indicates the liquid $NaNO_3$, while the blue portion is the solid $NaNO_3$. The black lines in the right part demonstrate the streamlines. It can be seen that the melted $NaNO_3$ close to the inner wall rises upward to the top of the capsule and absorbs heat from the wall. Meanwhile, the fluid at the top is driven downward along the surface of the solid phase. Therefore, cycling vortex and natural convection arise and become larger with the increasing liquid phase. As the liquid phase is hotter at the top, the solid $NaNO_3$ at the top melts faster than that at the bottom. In addition, as shown in Fig. 3, at the bottom some smaller vortexes are formed and recirculate between the bottom of solid phase and the capsule shell, resulting that the bottom solid melts quicker than that of the left and right sides. Due to the buoyancy-driven convection, the liquid-solid interface is not round. These phenomena are similar to the results presented in Tan [8] and Fan et al. [10].

5 min   15 min   25 min

Fig. 3 The evaluation of the liquid fraction (left) and the streamlines (right) of the NaNO$_3$.

To check whether the previously mentioned equations for the effective thermal conductivity can be used to simulate the melting process, Eqs. (2-6) are substituted into the conduction controlled model with the following equation:
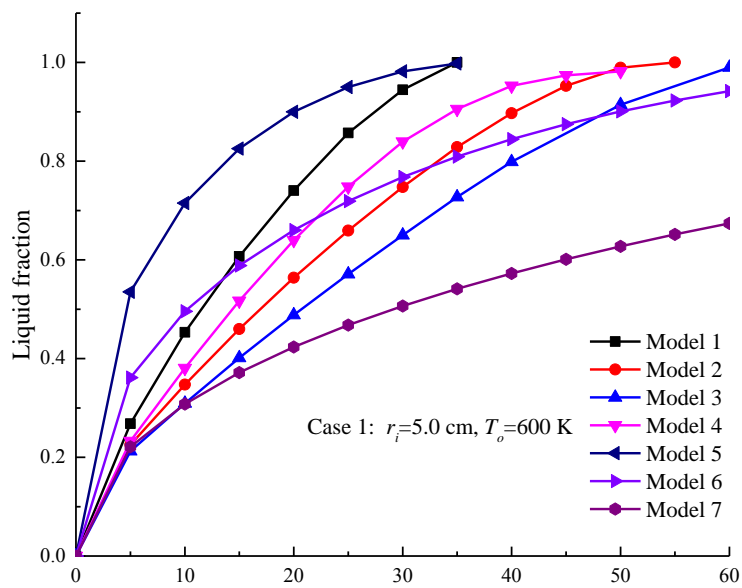
$$\rho C_p \frac{\partial T}{\partial t} = k_{eff} \left(\frac{\partial^2 T}{\partial x^2} + \frac{\partial^2 T}{\partial y^2} \right) - \rho \Delta H \frac{\partial f}{\partial t} \tag{13}$$

The characteristic length of the Rayleigh number for Eqs. (2-6) is the gap spacing δ between the solid-liquid interface and the inner surface of the capsule shell, and is changing during the melting process.

Table 3 lists the governing equations and the thermal conductivity for melted PCM of all the models used in this section. Models 2-6 are the conduction controlled models with different effective thermal conductivity correlations, while Model 7 uses the original PCM thermal conductivity as the effective thermal conductivity, which means that the natural convection effect is not considered in Model 7.

Table 3 Governing equations and thermal conductivity for melted PCM of each model.

	Governing equations	Thermal conductivity
Model 1	Eqs. (7-12)	original PCM conductivity
Model 2	Eq. 13	Eq. 2
Model 3	Eq. 13	Eq. 3
Model 4	Eq. 13	Eq. 4
Model 5	Eq. 13	Eq. 5
Model 6	Eq. 13	Eq. 6
Model 7	Eq. 13	original PCM conductivity

Case 1: r_i=5.0 cm, T_o=600 K

Legend:
- Model 1
- Model 2
- Model 3
- Model 4
- Model 5
- Model 6
- Model 7

Y-axis: Liquid fraction

To further compare the results of Models 1-7 under different geometric and boundary conditions, five other cases (Cases 2-6) are investigated. Table 4 shows the values of r_i and T_o of these five cases.

Table 4 The values of r_i, and T_o for Cases 2-6.

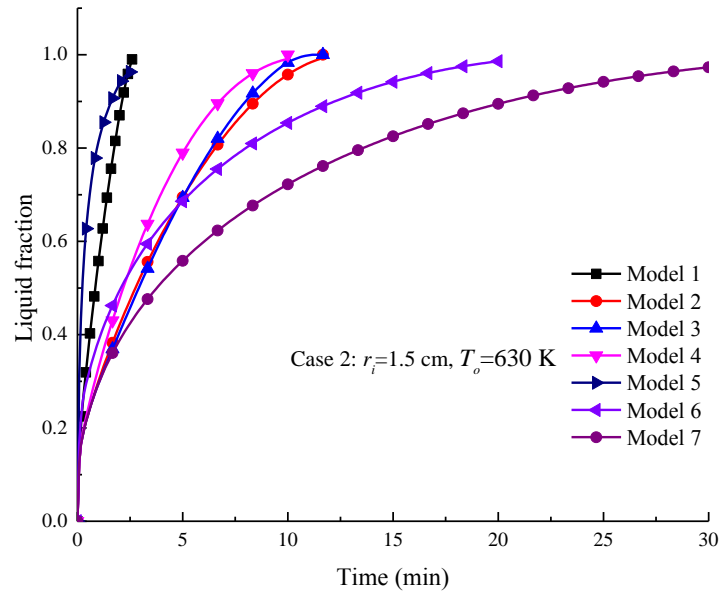| Case No.	r_i (cm)	T_o (K)
Case 2	1.5	630
Case 3	2.5	645
Case 4	5.0	615
Case 5	5.0	645
Case 6	8.0	645

Fig. 5 Comparison of the change of the liquid fraction among Models 1-7 (Case 2).
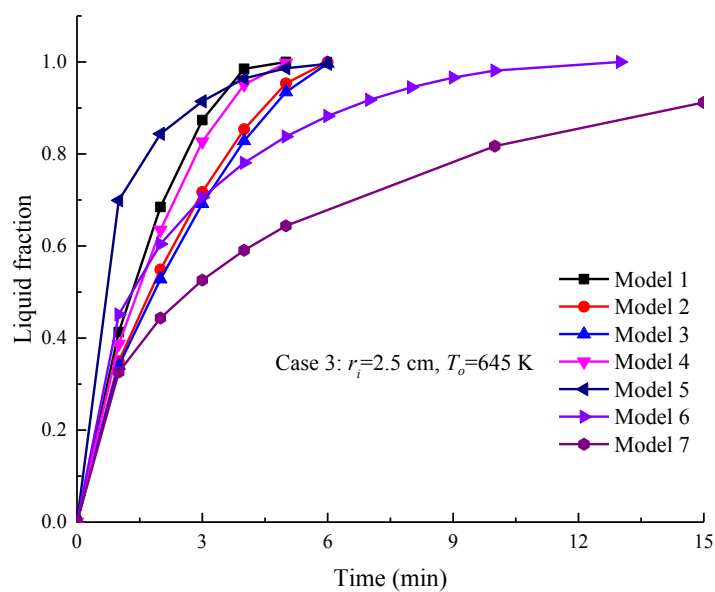
Fig. 6 Comparison of the change of the liquid fraction among Models 1-7 (Case 3).
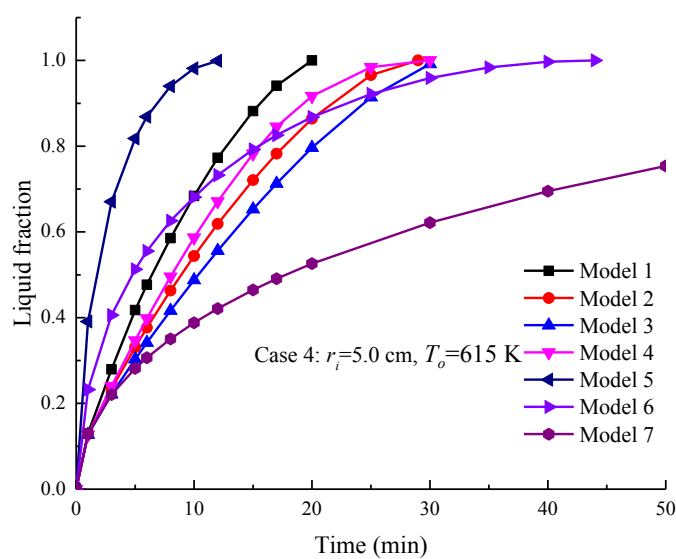

Fig. 7 Comparison of the change of the liquid fraction among Models 1-7 (Case 4).
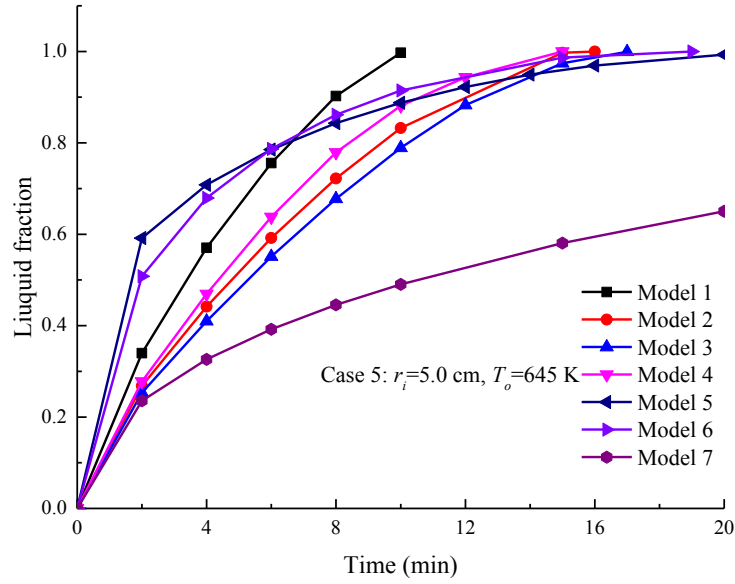
Fig. 8 Comparison of the change of the liquid fraction among Models 1-7 (Case 5).
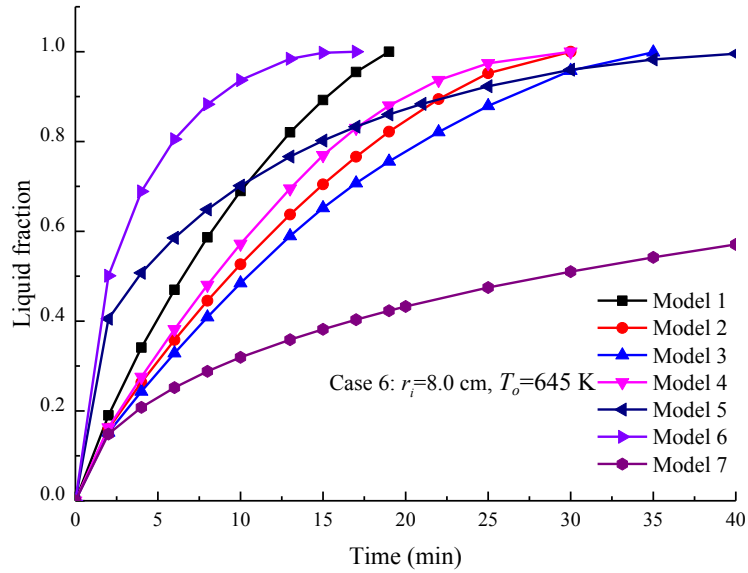

Fig. 9 Comparison of the change of the liquid fraction among Models 1-7 (Case 6).

Figures 5-9 show the variation of liquid fraction for Cases 2-6 calculated by Models 1-7. Fig. 5 shows that the liquid fraction predicted from Model 1 is lower than that from Model 5 but higher than that from other models. Similar to Fig. 4, Models 2-4 always

present a lower liquid fraction in Figs. 6-9 and Model 4 shows the closest result to Model 1. Model 7 in Figs. 6-9 always presents the slowest increase of liquid fraction. In Figs. 6-7, the liquid fraction calculated by Model 5 is higher than that by Model 1 during the melting process, but in Figs. 8 and 9, Model 5 gives a higher liquid fraction initially and then a lower liquid fraction. In Figs. 6-8, the liquid fraction predicted by Model 6 is higher than that by Model 1 at the beginning and becomes lower in the latter period, but in Fig. 9, Model 6 presents a higher liquid fraction through the whole process. It can be concluded that the liquid fractions predicted by Models 2-6 substantially deviate from that by Model 1 for the six cases. This could be due to the fact that the reported effective thermal conductivity correlations in Models 2-7 have their own validated ranges and are not developed for the melting process in a capsule as mentioned in the Introduction section.

Therefore, it is essential to deduce a new effective thermal conductivity correlation for PCM melting in a capsule. During the melting process simulated by Model 1, the instant heat flux Q transferring from the capsule shell to $NaNO_3$ can be calculated as:

$$Q = \frac{\overline{T}_{interface} - T_m}{R_{eff}} \tag{14}$$

in which $\overline{T}_{interface}$ is the average temperature of the inner wall of the capsule shell, R_{eff} is the effective thermal resistance and can be expressed as:

$$R_{eff} = \frac{1}{k_{eff}} \frac{1}{4\pi} \left(\frac{1}{\overline{r}_{interface}} - \frac{1}{r_i} \right) \tag{15}$$

where $\overline{r}_{interface}$ is the equivalent radius of the unmelted solid phase based on the mass conversation, and it can be calculated by:

18

$$\bar{r}_{interface} = \sqrt[3]{1 - l_f}\, r_i \tag{16}$$

where l_f is the liquid mass fraction of $NaNO_3$ in the capsule. Once Q and l_f are obtained, the effective thermal conductivity can be calculated by Eqs. (14-16). Based on all the six cases discussed above, Rayleigh number vs. the effective thermal conductivity calculated from Eqs. (14-16) is showed in Fig. 10 with logarithmic coordinates. By linear regression, the effective thermal conductivity can be expressed as follows:

$$\frac{k_{eff}}{k} = 0.174 Ra_\delta^{0.323} \qquad 10^3 < Ra_\delta < 5 \times 10^8 \tag{17}$$

for which the adjusted R-squared is 0.95. The flow inside the capsule for the condition with higher Ra_δ ($>10^9$) will become turbulence, which is beyond the scope of present study.
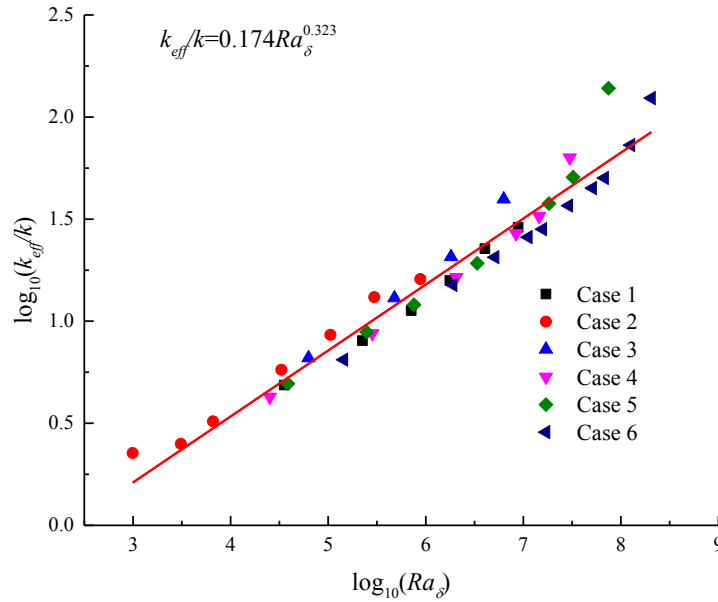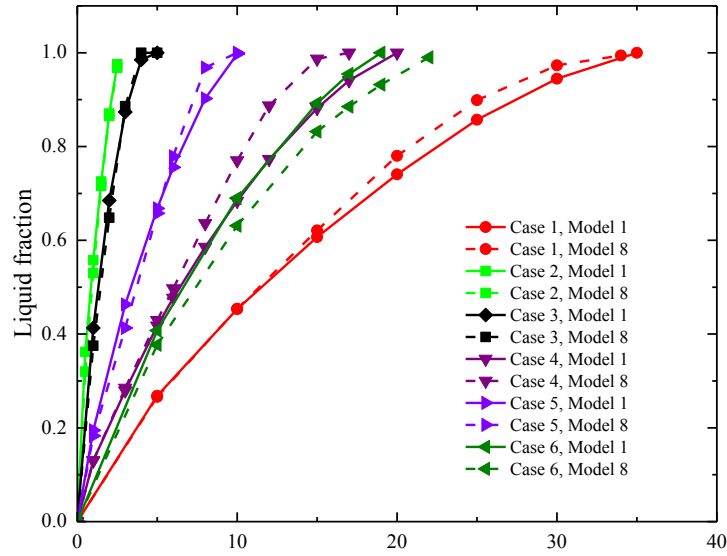

Fig. 10 The relationship between the Rayleigh number and the effective thermal conductivity.

19

	Case 1	Case 2	Case 3	Case 4	Case 5	Case 6
Model 1	N/A	N/A	N/A	N/A	N/A	N/A
Model 2	21%	45%	14%	17%	20%	21%
Model 3	30%	46%	17%	24%	25%	27%
Model 4	13%	39%	5%	12%	15%	16%
Model 5	33%	41%	21%	85%	24%	27%
Model 6	16%	31%	16%	21%	17%	57%
Model 7	38%	47%	35%	36%	46%	49%
Model 8	2%	3%	4%	7%	5%	7%

To check the accuracy of the proposed correlation (Eq. 17), the conduction controlled model with Eq. 17 as the effective thermal conductivity correlation (termed as

Model 8) is used to simulate Cases 1-6. Fig. 11 presents the comparison of the change of liquid fraction between Model 1 and Model 8 for Cases 1-6. As can be seen, the results of Model 8 are in good agreement with Model 1. Table 5 gives the averages of the absolute values of the relative difference between the liquid fractions calculated from Models 2-8 and from Model 1 for Cases 1-6 during the melting process. It can be clearly seen that Model 8, which uses the newly proposed effective thermal conductivity correlation (Eq. 17), yields the results closest to that of Model 1. The averages of the absolute values of the relative difference between Model 8 and Model 1 are smaller than 10% for all the six cases. Therefore, better than the above mentioned correlations in the literature, the proposed effective thermal conductivity correlation can be well used in the conduction controlled model to simulate the constrained melting of a capsule as well as the melting process of PCM capsules in a packed bed TES system in a simple way.

4. Conclusion

In the present study, the constrained melting of the $NaNO_3$ in a spherical capsule with different conditions are simulated by a validated natural convection included model and the conduction controlled model with five different reported formulas of the effective thermal conductivity. It is found that the results from the natural convection included model and the conduction controlled model with the reported effective thermal conductivity formulas show obvious discrepancy. This indicates that the reported correlations cannot correctly present the natural convection inside the capsule during the melting process. From that point, a novel effective thermal conductivity correlation is proposed based on the simulated results from the natural convection included model. The results show that the relative difference between the natural convection included model

and the conduction controlled model using the newly proposed effective thermal conductivity correlation can be decreased significantly to smaller than 10% for the Rayleigh number ranging from 10^3 to 5×10^8. Therefore, the proposed correlation for the effective thermal conductivity in the present study can be well used in simulating the melting process of PCM capsules in the field of packed bed latent heat energy storage.

Acknowledgments

Nomenclature

c_p	thermal capacity, J kg^{-1} K^{-1}
d	diameter, cm
f	liquid fraction
g	gravity, kg m^{-1} s^{-1}
Gr	Grashof number
k	thermal conductivity, W m^{-1} K^{-1}
L	length, m
Pr	Prandtl number
Ra	Rayleigh number
r	radius, cm

u	x-direction velocity, m s^{-1}
v	y-direction velocity, m s^{-1}
P	pressure, Pa
T	temperature, K

Greek

α	thermal diffusion coefficient, m^2 s^{-1}
β	thermal expansion coefficient, K^{-1}
δ	gap spacing, m
ΔH	latent heat, J kg^{-1}
μ	dynamic viscosity, Pa s
ν	kinematic viscosity, m^2 s^{-1}
ρ	density, kg m^{-3}

Subscripts

eff	effective
i	inner surface of the convection flow
ref	reference
s	solidus, solidus
o	outer surface of the convection flow
l	liquidus
m	melting
pcm	phase change material
w	wall

23

Reference

[1] S. Kuravi, J. Trahan, D.Y. Goswami, M.M. Rahman, E.K. Stefanakos. Thermal energy storage technologies and systems for concentrating solar power plants. Prog Energy Combust. 39 (2013) 285-319.
[2] H. Zhang, J. Baeyens, G. Cáceres, J. Degrève, Y. Lv. Thermal energy storage: Recent developments and practical aspects. Prog Energy Combust. 53 (2016) 1-40.
[3] B. Xu, P. Li, C. Chan, E. Tumilowicz. General volume sizing strategy for thermal storage system using phase change material for concentrated solar thermal power plant. Appl Energy. 140 (2015) 256-68.
[4] A. Gil, M. Medrano, I. Martorell, A. Lázaro, P. Dolado, B. Zalba, et al. State of the art on high temperature thermal energy storage for power generation. Part 1—Concepts, materials and modellization. Renew Sust Energy Rev. 14 (2010) 31-55.
[5] L. Xia, P. Zhang, R.Z. Wang. Numerical heat transfer analysis of the packed bed latent heat storage system based on an effective packed bed model. Energy. 35 (2010) 2022-32.
[6] N.S. Dhaidan, J.M. Khodadadi. Melting and convection of phase change materials in different shape containers: A review. Renew Sust Energy Rev. 43 (2015) 449-77.
[7] F.L. Tan, S.F. Hosseinizadeh, J.M. Khodadadi, L. Fan. Experimental and computational study of constrained melting of phase change materials (PCM) inside a spherical capsule. Int J Heat Mass Transfer. 52 (2009) 3464-72.
[8] F.L. Tan. Constrained and unconstrained melting inside a sphere. Int Commun Heat Mass. 35 (2008) 466-75.
[9] S.F. Hosseinizadeh, A.A. Rabienataj Darzi, F.L. Tan, J.M. Khodadadi. Unconstrained melting inside a sphere. Int J Thermal Sci. 63 (2013) 55-64.
[10] L. Fan, Z. Zhu, S. Xiao, M. Liu, H. Lu, Y. Zeng, et al. An experimental and numerical investigation of constrained melting heat transfer of a phase change material in a circumferentially finned spherical capsule for thermal energy storage. Appl Therm Eng. 100 (2016) 1063-75.
[11] J.M. Khodadadi, Y. Zhang. Effects of buoyancy-driven convection on melting within spherical containers. Int J Heat Mass Transfer. 44 (2001) 1605-18.
[12] J. Bedecarrats, F. Strub, B. Falcon, J. Dumas. Phase-change thermal energy storage using spherical capsules: performance of a test plant. Int J Refrig. 19 (1996) 187-96.
[13] K.A. Ismail, J. Henriquez, T. Da Silva. A parametric study on ice formation inside a spherical capsule. Int J Thermal Sci. 42 (2003) 881-7.
[14] N.A.M. Amin, F. Bruno, M. Belusko. Effective thermal conductivity for melting in PCM encapsulated in a sphere. Appl Energy. 122 (2014) 280-7.
[15] S. Karthikeyan, G. Ravikumar Solomon, V. Kumaresan, R. Velraj. Parametric studies on packed bed storage unit filled with PCM encapsulated spherical containers for low temperature solar air heating applications. Energy Convers Manage. 78 (2014) 74-80.
[16] S. Bellan, J. Gonzalez-Aguilar, M. Romero, M.M. Rahman, D.Y. Goswami, E.K. Stefanakos. Numerical Investigation of PCM-based Thermal Energy Storage System. Energy Proc. 69 (2015) 758-68.
[17] G. Raithby, K. Hollands. A general method of obtaining approximate solutions to laminar and turbulent free convection problems. Adv Heat Trans. 11 (1975) 265-315.
[18] M. Wu, C. Xu, Y.L. He. Cyclic behaviors of the molten-salt packed-bed thermal storage system filled with cascaded phase change material capsules. Appl Therm Eng. 93 (2016) 1061-73.
[19] M. Wu, C. Xu, Y.L. He. Dynamic thermal performance analysis of a molten-salt packed-bed thermal energy storage system using PCM capsules. Appl Energy. 121 (2014) 184-95.
[20] J. Scanlan, E. Bishop, R. Powe. Natural convection heat transfer between concentric spheres. Int J Heat Mass Transfer. 13 (1970) 1857-72.

[21] S. Kalaiselvam, R. Parameshwaran, S. Harikrishnan. Analytical and experimental investigations of nanoparticles embedded phase change materials for cooling application in modern buildings. Renew Energy. 39 (2012) 375-87.

[22] J.P. Holman. Heat transfer. McGraw-hill2010.

[23] M. Veerappan, S. Kalaiselvam, S. Iniyan, R. Goic. Phase change characteristic study of spherical PCMs in solar energy storage. Sol Energy. 83 (2009) 1245-52.

[24] N. Weber, R. Powe, E. Bishop, J. Scanlan. Heat transfer by natural convection between vertically eccentric spheres. J Heat Transfer. 95 (1973) 47-52.

[25] C.P. Chiu, W.R. Chen. Transient natural convection heat transfer between concentric and vertically eccentric spheres. Int J Heat Mass Transfer. 39 (1996) 1439-52.

[26] H.A. Adine, H. El Qarnia. Numerical analysis of the thermal behaviour of a shell-and-tube heat storage unit using phase change materials. Appl Math Model. 33 (2009) 2132-44.

[27] K. Pielichowska, K. Pielichowski. Phase change materials for thermal energy storage. Prog Mater Sci. 65 (2014) 67-123.

[28] V. Voller, M. Cross, N. Markatos. An enthalpy method for convection/diffusion phase change. Int J Numer Meth Eng. 24 (1987) 271-84.

[29] T. Bauer, D. Laing, R. Tamme. Characterization of sodium nitrate as phase change material. Int J Thermophys. 33 (2012) 91-104.

[30] G. Wei, G. Wang, C. Xu, X. Ju, L. Xing, X. Du, et al. Selection principles and thermophysical properties of high temperature phase change materials for thermal energy storage: A review. Renew Sust Energy Rev. (2017) https://doi.org/10.1016/j.rser.2017.05.271.

Highlights

1. A validated numerical model was used to simulate the melting process in a capsule.

2. The effective thermal conductivity correlations in the literature was discussed.

3. A new effective thermal conductivity correlations was proposed.

4. The proposed correlations shows better results than the reported correlations.